Creation and dynamics of remote spin-entangled pairs in the expansion of strongly correlated fermionic atom clouds

Stefan Keßler[1], Ian P. McCulloch[2], and Florian Marquardt[1,3]

[1]Institute for Theoretical Physics, Universität Erlangen-Nürnberg, Staudtstr. 7, 91058 Erlangen, Germany
[2]Centre for Engineered Quantum Systems, School of Mathematics and Physics, The University of Queensland, St Lucia, QLD 4072, Australia
[3]Max Planck Institute for the Science of Light, Günther-Scharowsky-Straße 1/Bau 24, 91058 Erlangen, Germany

Abstract. We consider the nonequilibrium dynamics of an interacting spin-$\frac{1}{2}$ fermion gas in a one-dimensional optical lattice after switching off the confining potential. In particular, we study the creation and the time evolution of spatially separated, spin-entangled fermionic pairs. The time-dependent density-matrix renormalization group is used to simulate the time evolution and evaluate the two-site spin correlation functions, from which the concurrence is calculated. We find that the typical distance between entangled fermions depends crucially on the onsite interaction strength, and that a time-dependent modulation of the tunneling amplitude can enhance the production of spin-entanglement. Moreover, we discuss the prospects of experimentally observing these phenomena using spin-dependent single-site detection.

Contents

1. Introduction

1.1. Motivation

The tremendous experimental progress with ultra cold atoms in optical lattices makes them a unique playground for studying nonequilibrium dynamics of many-body systems. The remarkable features of these systems are the precise and dynamical control of the interparticle interaction and external trapping potentials, as well as long coherence times [1]. Different nonequilibrium initial states can be generated by a quantum quench (for a recent review see [2]): a parameter in the Hamiltonian is suddenly changed such that the system, initially in the ground state of the Hamiltonian, is afterwards in an exited state of the new Hamiltonian. Quenches have been experimentally realized, for instance, in the interaction strength [3, 4, 5] and in the additional trapping potential by either switching it off [6] or displacing its center [7, 8, 9]. This led to observations such as the collapse and revival of the coherence in a Bose-Einstein condensate after a quench from the superfluid to the Mott insulating regime [3].

New detection schemes [10, 11, 12] provide the possibility of observing the many-body state at the single-site and single-atom level and make these systems even more suitable for studying the dynamics of (spatial) correlations in nonequilibrium

situations. These methods have already been used to monitor the propagation of quasi-particle pairs [13, 14] and a single spin impurity [15] in a bosonic gas. They have also inspired theoretical work on many-body dynamics subject to observations, treating issues such as entanglement growth in a bosonic system [16], destructive single-site measurements [17], and Quantum Zeno effect physics for spin [18] and expansion [19] dynamics.

In the present article, we study a different aspect of these systems: the creation and dynamics of spin-entanglement during the expansion of a strongly interacting, spin-balanced fermionic gas in an optical lattice. We find that the expansion out of an initial cluster of fermions can automatically generate long-range spin-entanglement.

Expansion dynamics of interacting fermions in an optical lattice has been realized recently in a three-dimensional optical lattice [6]. In that experiment, the authors observed a bimodal expansion with a ballistic and diffusive part and were able to explain its anomalous behaviour using a Boltzmann-based approach. In addition, expansion dynamics of this kind has been studied numerically in one dimension, going beyond a kinetic description. These studies revealed the dependence of the expansion velocity [20, 21], the momentum distribution function, and the spin and density structure factors [22] on the onsite interactions and the initial filling. Furthermore, the effects of the different quench scenarios [23] and of the gravitational field [24] on the time-evolution of the density distribution have been discussed. The sudden expansion of a spin-imbalanced fermionic gas has been recently considered for observing Fulde-Ferrell-Larkin-Ovchinnikov correlations [25, 26, 27].

In general, the dynamics is crucially affected by the difference in behaviour between a single fermion and that of a doublon (i.e., a pair of fermions at the same lattice site). For large interaction strengths doublons are very stable against decay into fermions (analogously to the repulsively bound boson pairs [28]) and move slowly. These properties can lead to the condensation of doublons [29] and a decrease of the entropy [30] in the center of the cloud during the expansion. In the present work, we will show how spin-entanglement is generated by the decay of a doublon into single fermions.

The article is organized as follows: First, we will describe in detail the expansion protocol, starting from a finitely extended band insulating state, i.e., a cluster of spin-singlet doublons. Moreover, we give details about the numerical time-dependent density matrix renormalization group (tDMRG) simulation. Before studying spin-physics, we first discuss correlations in the density of the expanding cloud (section 2), where the influence of interactions is already significant. We find that large onsite interactions lead to positive correlations between certain lattice sites. The dynamics of spin-entangled pairs, the main focus of our work, is then presented in section 3. First of all, we relate the concurrence to the spin-spin correlation functions. Then we discuss the propagation of spin-entangled pairs in the cloud. Furthermore, we compare the cumulative "amount" of spin-entanglement in different regions of the cloud and for various interaction strengths. We find that spin-entanglement between remote lattice sites is only found for large interaction strength, while for small onsite-interactions there is entanglement preferentially only between nearby sites. Moreover, the Pauli-blocked core of the cluster favours both partners of a spin-entangled pair to be emitted into the same direction when compared to the decay of a single doublon, where they almost always are emitted into different directions. In addition, we discuss the expansion under the action of a time-dependent (modulated) tunneling amplitude. We find that the modulation can enhance the production of spin-entanglement. Finally, we
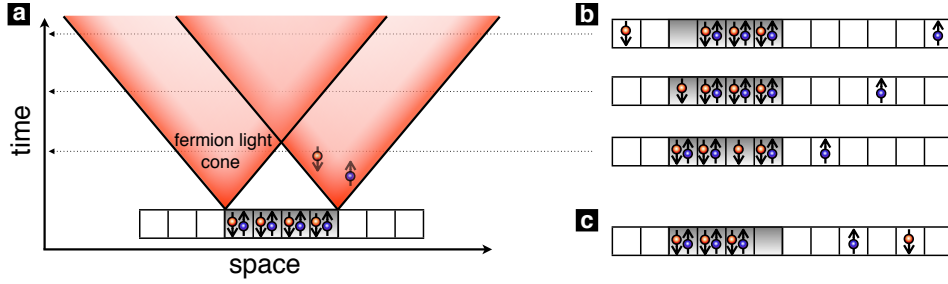
Figure 1. Schematic of the expansion from a band insulating initial state into an empty one-dimensional lattice. (a) Due to the discreteness of the lattice the velocity of the fermions is bounded. Thus, the fermions emitted from a doublon move within a light cone (shown for the leftmost and rightmost doublon). (b,c) Examples of fermion configurations at different evolution times, where only the rightmost doublon decayed into single fermions and the other doublons remained at the original position. (b) A spin up (down) excitation can propagate through the band insulating cluster as a spin down (up) hole (time evolution from bottom to top). (c) In this case, both fermions have been emitted to the same direction.

discuss a possible experimental setup for observing this spin-entanglement dynamics in the near future using spin-dependent single-site detection (section 4).

1.2. Model

In this paper, we consider an ultracold gas of fermionic atoms loaded into a one-dimensional optical lattice. The atoms can be prepared in two different hyperfine states, which we label ↑ and ↓, and fermions of different "spin" interact via s-wave scattering. This fermionic mixture represents a realization of the standard fermionic Hubbard Hamiltonian [31, 32]

$$\hat{\mathcal{H}} = -J \sum_{i=1}^{L-1} \sum_{a=\uparrow,\downarrow} \left\{ \hat{c}_{i,a}^\dagger \hat{c}_{i+1,a} + \hat{c}_{i+1,a}^\dagger \hat{c}_{i,a} \right\} + U \sum_{i=1}^{L} \hat{n}_{i,\uparrow} \hat{n}_{i,\downarrow}. \qquad (1)$$

The first term describes the tunneling of fermions between adjacent lattices sites with amplitude J. The second term encodes the effective onsite interaction energy U of fermions with different hyperfine states, which can be controlled using a Feshbach resonance. The particle number operator is $\hat{n}_{i,a} = \hat{c}_{i,a}^\dagger \hat{c}_{i,a}$, with the creation (annihilation) operator $\hat{c}_{i,a}^\dagger (\hat{c}_{i,a})$ satisfying the fermionic commutation relations.

In the following, we focus on the expansion from a band-insulating state, i.e., the sites in the center of the lattice are doubly occupied. Experimentally, this is achieved by using an additional trapping potential to confine the fermions to a central region of the optical lattice [6]. At time $t = 0$ the trapping potential is switched off and the fermions expand into the empty lattice sites, as depicted in figure 1(a).

The time evolution of the average fermion density and the average doublon density has already been studied for this expansion protocol, by numerical simulations for 1D lattices [20]. For large onsite interactions strengths $U/J \gtrsim 4$ two wave fronts with different velocities are visible in the time-dependent density profile, while there is a single wave front for small onsite interaction strengths. It turns out that the expansion can be basically understood as a mixture of propagating single fermions and doublons, see also [21]. For small onsite interaction strengths the initial state

quickly decays into single fermions, which move ballistically through the lattice. Due to the cosine dispersion relation of a single particle in the lattice, $\epsilon_k = -2J\cos(k)$ with wavenumber $k \in (-\pi, \pi]$, its maximal velocity is given by $|v_{max}| = 2J$. This fact leads to light cones in the density distribution, as indicated in figure 1(a). For large onsite interaction $U/J \gtrsim 4$, only a small fraction of doublons decay into fermions, which move away ballistically. As the effective tunneling amplitude of a doublon is $2J^2/U$, they initially remain in the central region and then move through the lattice on a much larger time scale.

However, the propagation of the single fermions is highly correlated, as they are always created as spin-singlet pair when a doublon decays. As sketched in figures 1(b) and (c), the two particles of such a spin-entangled pair may be either detected on the same side of the initial cluster or on different sides.

We briefly point out that the dynamics of the spin-entanglement as well as that of the density-density correlation is invariant under the change of the sign in the interaction strength U. This is a direct consequence of a transformation property of the (spin- or density-) correlators and of the initial state under time reversal and π-boost (translation of all momenta by π). This dynamical $U \mapsto -U$ symmetry in the Hubbard model is discussed in more detail in [6, 33].

1.3. Numerical simulation

For the numerical evaluation of the nonequilibrium time evolution, we employ the time-dependent density-matrix renormalization group (tDMRG) method [34, 35, 36, 37, 38]. The initial state is a cluster consisting of 10 doublons, which are located in the center of a lattice of size $L = 100$ with open boundary conditions. Our tDMRG simulation uses a Krylov subspace method with time step $J\delta t = 0.125$ and the discarded weight is set to either 10^{-5} or 10^{-6}, depending on the interaction strength. For all evolution times shown in the figures, the density remains negligible at the boundaries of the lattice. We also verified that the features presented here does not dependent on the precise position of the cluster in the lattice nor change when the truncation error is modified within the given range.

For non-interacting particles, we have used the exact expressions for the time-dependent correlation functions and concurrence, as given in appendix A.

2. Density-density correlation

Before turning to the spin-entanglement (in the subsequent section), we will first study the density-density correlation function $D_{ij}(t) = \langle \hat{n}_i(t)\hat{n}_j(t) \rangle - \langle \hat{n}_i(t) \rangle \langle \hat{n}_j(t) \rangle$, with $\hat{n}_i = \hat{n}_{i,\uparrow} + \hat{n}_{i,\downarrow}$. For the expansion, sketched in figure 1, the density at different lattice sites is expected to be correlated for several reasons, in particular since the fermions are always created in pairs out of doublons.

Note that the single-site detection of density correlations (more precisely the parity correlations) has been very recently used to study the quasi-particle propagation in a commensurate ultracold bosonic gas after an interaction quench [13, 14]. It has also been employed to study the role of onsite interaction in a bosonic two-body quantum walk, experimentally realized in a nonlinear optical waveguide lattice [39].

As a point of reference, we first consider the density-density correlations for the initial state consisting of a single doublon. The fluctuation in the density at a lattice site i, $D_{ii}(t)$, is the variance of the occupation number $\hat{n}_i$. For the expansion from a
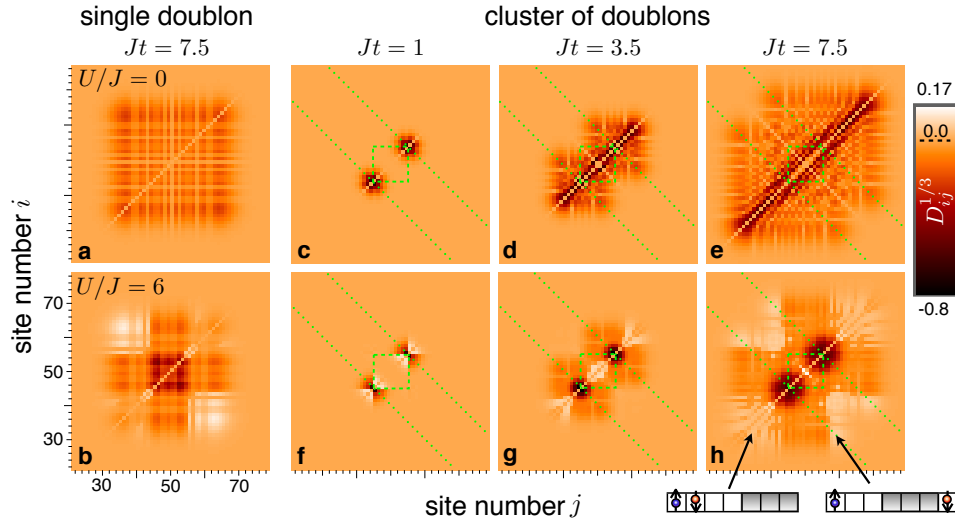
Figure 2. Off-diagonal density correlations $D_{i,j\neq i}(t) = \langle\hat{n}_i(t)\hat{n}_{j\neq i}(t)\rangle - \langle\hat{n}_i(t)\rangle\langle\hat{n}_{j\neq i}(t)\rangle$ for the expansion from an initial state consisting of a single doublon (a,b) and a cluster of ten doublons (c-h). For better visibility we display the values of $D_{ij}^{1/3}$ as a colour scale and set D_{ii} to zero. (c,f) Initially all fermions but the outermost ones are Pauli-blocked. This leads to non-vanishing density-density correlations only close to the edge of the initial configuration for small evolution times. (a,c-e) For vanishing onsite interaction U, the density-density correlation equals the two-site spin-z correlation and is always nonpositive, cf. equations (A.5) and (A.7). (b,f-h) In the interacting case, the density-density correlation can be positive. (b) For a single doublon, $D_{i,j\neq i}(t) > 0$ only for i and j at different sides of the initially occupied lattice site. Thus, the doublon decays primarily into fermions moving in opposite directions. (f-h) For a cluster of doublons, positive density correlations are also found for lattice sites i and j that are both located to the left or to the right of the initial cluster position, or within the initial cluster (indicated by the dashed square).

doublon, it is maximal for those lattice sites located at the edge of the single fermion light cone (doublon light cone) in the noninteracting (strongly interacting) case. In the following we focus on the off-diagonal density-density correlations $D_{ij\neq i}(t)$, which are shown in figures 2(a) and (b). Most importantly, we find that the onsite interaction U leads to a positive correlation of those fermions propagating with almost maximal velocity $|2J|$ in opposite directions, see figure 2(b). On the other hand, the density-density correlation assumes large negative values between those lattice sites in the center that are most likely occupied by the doublon (and not by single fermions) [central square region in figure 2(b)]. In contrast, the off-diagonal density-density correlations are always nonpositive for clusters of noninteracting fermions, as detailed in appendix A, see also figures 2(a) and (c)-(e).

The bunching effect in the interacting case can be understood by writing the motion of the two fermions in relative and center of mass coordinates, r and R, respectively (see appendix B for details of the discussion). Note that we assume an infinite lattice for this argument, which is compatible with the simulation as the boundary conditions do not play a role for the evolution times considered here. The

center of mass motion is a plane wave with total wavenumber $K = (k_1 + k_2) \bmod 2\pi$, where k_1 and k_2 are the asymptotic wave numbers of the single fermions. The relative motion is described by a K-dependent Hamiltonian. For $U \neq 0$, the eigenstates of this Hamiltonian are one bound state and scattering states. The probability for the doublon to decay into one specific scattering state with wavefunction $\psi_{K,k}(r)$ [where $k = (k_1 - k_2)/2$ is the relative wavenumber] is given by the modulus squared of that wavefunction's probability amplitude at $r = 0$: $|\psi_{K,k}(0)|^2$. This decay probability is, up to an overall normalization constant [see equation (B.5)]:

$$|\psi_{K,k}(0)|^2 \propto \left[1 + U^2 / \left(16J^2 \cos^2(K/2)\sin^2(k)\right)\right]^{-1}. \tag{2}$$

For small onsite interactions $|U/4J| \ll 1$, the decay probability is almost the same for the different scattering states, except for $K \approx \pi$ or $k \approx 0$ where it drops to zero. In the strongly interacting case, it exhibits a pronounced maximum for $K = 0$ and $k = \pm\pi/2$, that is $k_1 = \pm\pi/2$ and $k_2 = \mp\pi/2$. In other words, for large onsite interaction the doublon decays primarily into two fermions moving in opposite directions with velocity close to $|2J|$.

Next we study the density correlations for the expansion from a cluster of several doublons into an empty lattice. The results are displayed in figures 2(c)-(h). Just as for the single doublon, the off-diagonal density correlation has regions of positive values in the presence of onsite interaction. However, in contrast to the case of a single doublon, the existence of other doublons now leads to positive correlations also at lattice sites located on the same side of the initial cluster, see figures 2(f)-(h). Positive correlations between sites on different sides of the cluster are only observed for evolution times larger than the time a hole takes to propagate through the cluster, cf. figure 2(h).

The results suggest that the initially Pauli blocked core of the cluster leads to an enhanced decay of the outermost doublons into single fermions moving away in the same direction. However, the alternative case, where the edge doublon decays into a fermion and a hole moving into the opposite direction close to the maximal velocity $|2J|$ also leads to positive correlations. Further simulations show that positive density correlations between lattice sites on the same side of the initial cluster positions are found for clusters of about four and more doublons and $U/J \gtrsim 2$. Note that as the single fermions are created by the decay of an edge doublon, the situation is different from a free single fermion or fermionic wave packet approaching a cluster of doublons. In the latter situations, the fermion is almost perfectly transmitted through the cluster (band insulating state) in the limit of large onsite interaction [40, 41].

In the next section, we discuss the spin-entanglement. This will reveal that the positive density correlations indeed stem from singlet pairs, which become delocalized by the decay of a doublon.

3. Spin-entanglement between different lattice sites within the expanding cloud

In this section, we discuss the entanglement between fermions located at different lattice sites by means of the concurrence [42]. First, the relation between the concurrence and the spin-spin correlations is established. Then we use tDMRG simulations to find the regions where fermions are likely and unlikely to be entangled during the expansion. We examine the role of the onsite interaction and the core of the cluster on the entanglement dynamics.

3.1. Reduced density matrix and concurrence of two fermions

In this paragraph we derive the reduced density matrix and the concurrence for fermions located at different lattice sites within the expanding cloud (see [43] for a related discussion in the context of solid state physics). Given the full many-body wavefunction $|\Psi(t)\rangle$, the reduced density matrix for the lattice sites i and j is $\hat{\rho}_{ij}(t) = \mathrm{Tr}_{\mathrm{sites}\neq i,j}\{|\Psi(t)\rangle\langle\Psi(t)|\}$, where all other lattice sites have been traced out. Whenever two fermions are situated at the same lattice site they form a spin-singlet pair as their spatial degrees of freedom are symmetric under particle exchange. Thus, entanglement in the spin degree of freedom between fermions at two different lattice sites can only occur if each lattice site is occupied by a single fermion. Projecting $\hat{\rho}_{ij}(t)$ onto those states yields

$$\hat{\rho}_{ij}^s(t) = \frac{1}{\mathrm{Tr}\{\hat{\rho}_{ij}(t)\,\hat{n}_i^s\hat{n}_j^s\}}\hat{n}_j^s\hat{n}_i^s\,\hat{\rho}_{ij}(t)\,\hat{n}_i^s\hat{n}_j^s. \tag{3}$$

Here, $\hat{n}_i^s = \hat{n}_{i,\uparrow} + \hat{n}_{i,\downarrow} - 2\hat{n}_{i,\uparrow}\hat{n}_{i,\downarrow}$ is the single fermion number operator at site i, which projects onto a subspace with exactly one fermion on that site. The normalization factor in the denominator, $\mathrm{Tr}\{\hat{\rho}_{ij}(t)\hat{n}_i^s\hat{n}_j^s\} = \langle\hat{n}_i^s(t)\hat{n}_j^s(t)\rangle$, is the probability of finding at time t a single fermion at each of the lattice sites i and j. The state described by $\hat{\rho}_{ij}^s(t)$ is the state obtained after a successful projective measurement. The reduced density matrix $\hat{\rho}_{ij}^s(t)$ is equivalent to a two-qubit density matrix, which can be expressed in the form $\hat{\rho} = \sum_{\alpha,\beta=0}^{3}\lambda^{\alpha\beta}\,\hat{\sigma}_{(1)}^\alpha\otimes\hat{\sigma}_{(2)}^\beta$, where $\hat{\sigma}^{1,2,3}$ are the Pauli matrices, $\hat{\sigma}^0 = \mathbf{1}$, and the factors $\lambda^{\alpha\beta}$ are determined by the correlation functions $\lambda^{\alpha\beta} = \frac{1}{4}\langle\hat{\sigma}_{(1)}^\alpha\hat{\sigma}_{(2)}^\beta\rangle$ [44]. Consequently, the reduced density matrix of single fermions at lattice sites i and j can be written as

$$\hat{\rho}_{ij}^s(t) = \frac{1}{\langle\hat{n}_i^s(t)\hat{n}_j^s(t)\rangle}\sum_{\alpha,\beta=0}^{3}\langle\hat{S}_i^\alpha(t)\hat{S}_j^\beta(t)\rangle\,\hat{\sigma}_i^\alpha\otimes\hat{\sigma}_j^\beta, \tag{4}$$

where $\hat{S}_i^{1,2,3} = \frac{1}{2}\sum_{a,b=\uparrow,\downarrow}\hat{c}_{i,a}^\dagger(\hat{\sigma}^{1,2,3})^a{}_b\hat{c}_{i,b}$ is the x-, y-, and z-component of the spin operator and $\hat{S}_i^0$ is, for compactness, defined as half the single fermion number operator, $\hat{S}_i^0 := \frac{1}{2}\hat{n}_i^s$. Note that $\langle\hat{S}_i^\alpha(t)\hat{S}_j^\beta(t)\rangle$ is calculated using the full (unprojected) wavefunction since states with vacancies or doublons at site i or j do not contribute to the expectation value.

Symmetries of the initial state and the Hamiltonian can simplify the form of the reduced density matrix, such that only a few correlation functions are needed to determine $\hat{\rho}_{ij}^s(t)$. As detailed now, the reduced density matrix $\hat{\rho}_{ij}^s(t)$ depends only on $\langle\hat{S}_i^z(t)\hat{S}_j^z(t)\rangle/\langle\hat{n}_i^s(t)\hat{n}_j^s(t)\rangle$ for the cluster initial state shown in figure 1. The Hubbard Hamiltonian (1) preserves the spin-dependent particle number, i.e., $[\hat{\mathcal{H}},\hat{N}_{\uparrow,\downarrow}] = 0$, $\hat{N}_{\uparrow,\downarrow} = \sum_{i=1}^{L}\hat{n}_{\uparrow,\downarrow}$. Given an initial state with fixed number of spin-up and spin-down fermions, which is the usually case in cold atom experiments, the time-dependent expectation values of operators that do change the spin-dependent particle number vanish. This yields $\langle\hat{n}_i^s(t)\hat{S}_j^{x,y}(t)\rangle = 0$, $\langle\hat{S}_i^{x,y}(t)\hat{S}_j^z(t)\rangle = 0$, and $\langle\hat{S}_i^x(t)\hat{S}_j^x(t)\rangle - \langle\hat{S}_i^y(t)\hat{S}_j^y(t)\rangle \pm i[\langle\hat{S}_i^x(t)\hat{S}_j^y(t)\rangle + \langle\hat{S}_i^y(t)\hat{S}_j^x(t)\rangle] = 0$. The latter condition comes from creating two spin-down (spin-up) fermions while destroying two spin-up (spin-down) fermions at lattice sites i and j and can also be written as $\langle\hat{S}_i^x(t)\hat{S}_j^x(t)\rangle = \langle\hat{S}_i^y(t)\hat{S}_j^y(t)\rangle$ and $\langle\hat{S}_i^x(t)\hat{S}_j^y(t)\rangle = -\langle\hat{S}_i^y(t)\hat{S}_j^x(t)\rangle$. Moreover, the Hamiltonian (1) is fully rotationally

invariant, $[\hat{\mathcal{H}}, \sum_{i=1}^{L} \hat{S}_i^{x,y,z}] = 0$. If the initial state is rotationally invariant, for instance a cluster of doublons, then the many-body state remains SU(2) spin symmetric during the time evolution. It follows that $\langle \hat{S}_i^z(t)\hat{S}_j^z(t)\rangle = \langle \hat{S}_i^x(t)\hat{S}_j^x(t)\rangle = \langle \hat{S}_i^y(t)\hat{S}_j^y(t)\rangle$, $\langle \hat{n}_i^s(t)\hat{S}_j^z(t)\rangle = \langle \hat{n}_i^s(t)\hat{S}_j^{x,y}(t)\rangle = 0$, and $\langle \hat{S}_i^x(t)\hat{S}_j^y(t)\rangle = \langle \hat{S}_i^{x,y}(t)\hat{S}_j^z(t)\rangle = 0$. In summary, the reduced density matrix for the expansion from a cluster of doublons reads

$$\hat{\rho}_{ij}^s(t) = \frac{1}{4} \cdot \mathbf{1} + \frac{\langle \hat{S}_i^z(t)\hat{S}_j^z(t)\rangle}{\langle \hat{n}_i^s(t)\hat{n}_j^s(t)\rangle} \left[\hat{\sigma}_i^x \otimes \hat{\sigma}_j^x + \hat{\sigma}_i^y \otimes \hat{\sigma}_j^y + \hat{\sigma}_i^z \otimes \hat{\sigma}_j^z \right]$$

$$= \left(\frac{1}{4} + \frac{\langle \hat{S}_i^z(t)\hat{S}_j^z(t)\rangle}{\langle \hat{n}_i^s(t)\hat{n}_j^s(t)\rangle} \right) \left[|T_{ij}^1\rangle\langle T_{ij}^1| + |T_{ij}^0\rangle\langle T_{ij}^0| + |T_{ij}^{-1}\rangle\langle T_{ij}^{-1}| \right]$$

$$+ \left(\frac{1}{4} - 3\frac{\langle \hat{S}_i^z(t)\hat{S}_j^z(t)\rangle}{\langle \hat{n}_i^s(t)\hat{n}_j^s(t)\rangle} \right) |S_{ij}\rangle\langle S_{ij}|, \tag{5}$$

where $|S_{ij}\rangle = \frac{1}{\sqrt{2}}(|\uparrow_i\downarrow_j\rangle - |\downarrow_i\uparrow_j\rangle)$ is the singlet state and $|T_{ij}^m\rangle$ is the triplet state with the m denoting the spin projection in z-direction.

Instead of $\langle \hat{S}_i^z(t)\hat{S}_j^z(t)\rangle$ one could in principle evaluate the spin-spin correlation in any other direction. However, for cold atomic gases in optical lattices the correlation function $\langle \hat{S}_i^z(t)\hat{S}_j^z(t)\rangle = \frac{1}{4}\langle[\hat{n}_{i,\uparrow}(t) - \hat{n}_{i,\downarrow}(t)][\hat{n}_{j,\uparrow}(t) - \hat{n}_{j,\downarrow}(t)]\rangle$ seems to be experimentally most realistic to access as it could be obtained from snapshots of the spin-dependent single-site detection of the particle number.

The spin-entanglement between single fermions can be derived from the reduced density matrix. In this work, we use the concurrence $C(\hat{\rho})$ [42] to quantify the entanglement. Given the time-reversed density matrix $\hat{\tilde{\rho}} = \sigma^y \otimes \sigma^y \hat{\rho}^* \sigma^y \otimes \sigma^y$, with the complex conjugation $\hat{\rho}^*$ taken in the standard basis $\{|\uparrow\uparrow\rangle, |\uparrow\downarrow\rangle, |\downarrow\uparrow\rangle, |\downarrow\downarrow\rangle\}$, the concurrence is defined by $C(\hat{\rho}) = \max\{0, \sqrt{\lambda_1} - \sqrt{\lambda_2} - \sqrt{\lambda_3} - \sqrt{\lambda_4}\}$, where the λ_i's are the eigenvalues of $\hat{\rho}\hat{\tilde{\rho}}$ in descending order. In our case, the concurrence of the reduced density matrix (5) is given by

$$C_{i,j}(t) = \max \left\{ 0, -\frac{1}{2} - 6\frac{\langle \hat{S}_i^z(t)\hat{S}_j^z(t)\rangle}{\langle \hat{n}_i^s(t)\hat{n}_j^s(t)\rangle} \right\}. \tag{6}$$

Spin-spin correlations $\langle \hat{S}_i^z(t)\hat{S}_j^z(t)\rangle/\langle \hat{n}_i^s(t)\hat{n}_j^s(t)\rangle \geq -1/12$ result in a vanishing concurrence. The concurrence approaches 1 as $\langle \hat{S}_i^z(t)\hat{S}_j^z(t)\rangle/\langle \hat{n}_i^s(t)\hat{n}_j^s(t)\rangle \searrow -1/4$, i.e., when the two fermions detected at lattice sites i and j always have opposite spin.

The probability that single fermions at lattice sites i and j form a spin-singlet pair can be directly read off the reduced density matrix (5):

$$P_{ij}^{Singlet}(t) = \text{Tr}\left[\hat{\rho}_{ij}^s(t)|\mathcal{S}_{ij}\rangle\langle\mathcal{S}_{ij}| \right] = \frac{1}{4} - 3\frac{\langle \hat{S}_i^z(t)\hat{S}_j^z(t)\rangle}{\langle \hat{n}_i^s(t)\hat{n}_j^s(t)\rangle}. \tag{7}$$

Each of the spin triplet states is measured with the probability $1/4 + \langle \hat{S}_i^z(t)\hat{S}_j^z(t)\rangle/\langle \hat{n}_i^s(t)\hat{n}_j^s(t)\rangle$.

3.2. Time evolution of the spin-entanglement within the expanding cloud

Spin-entanglement between different lattice sites, which we denote by i and j, requires that both sites are singly occupied as discussed in section 3.1. The probability for this is $\langle \hat{n}_i^s(t)\hat{n}_j^s(t)\rangle$, with the single fermion number operator already defined above
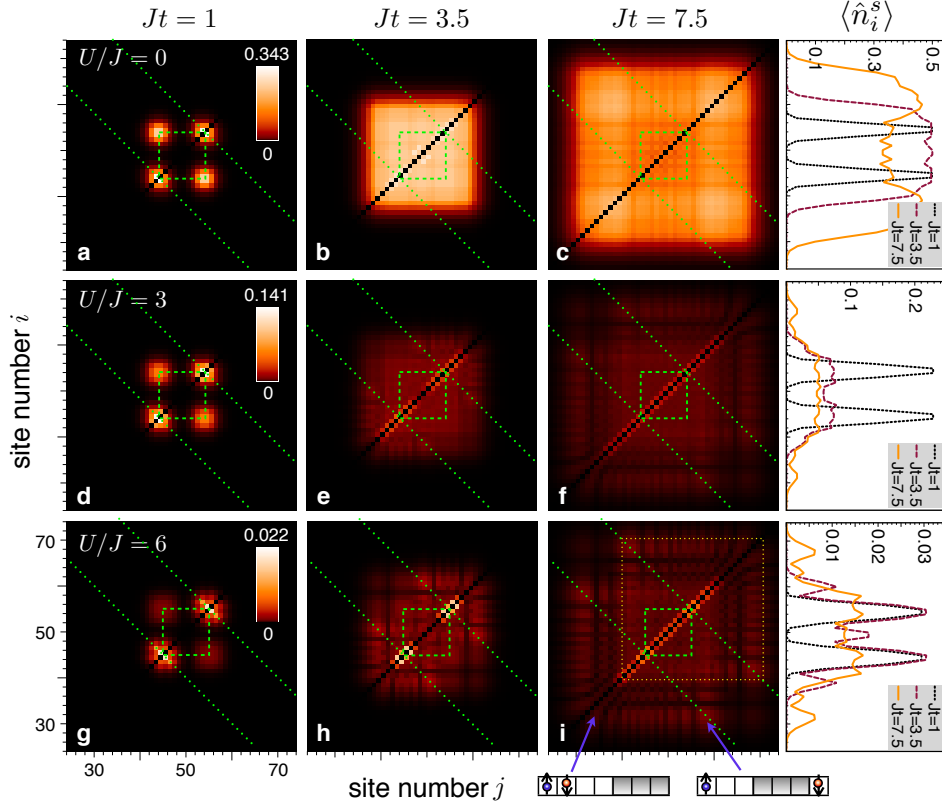
Figure 3. Density-density correlation of single fermions $\langle \hat{n}_i^s(t)\hat{n}_{j\neq i}^s(t)\rangle$ (i.e. excluding doublons) for the expansion from an initial cluster of doublons in one dimension (the initial position of the ten doublons is indicated by the dashed square). (a-c) Without onsite interactions, $U/J = 0$, the fermions move ballistically through the lattice. This is reflected by the fourfold symmetry of the correlation matrix shown here. (d-i) When increasing U/J, fermions are created only rarely by the decay of a doublon at the edge of the cluster. These two fermions move within the same light cone, cf. figure 1. The light cone leads to a square shape of the correlation function having its center at the edge of the initial cluster, shown by the dotted square in panel (i). The dotted lines indicate pairs of coordinates corresponding to fermions emitted with opposite velocities by a doublon at the edge of the cloud. Moreover, an increased correlation between nearest neighbor lattice sites is found for larger evolution times, see (f) and (i).

$(\hat{n}_i^s = \hat{n}_{i,\uparrow} + \hat{n}_{i,\downarrow} - 2\hat{n}_{i,\uparrow}\hat{n}_{i,\downarrow})$. Figure 3 shows the numerical results for $\langle \hat{n}_i^s(t)\hat{n}_{j\neq i}^s(t)\rangle$ for different evolution times Jt and onsite interaction strengths U/J.

Shortly after the quench, single fermions are created at the edges of the cluster, see figures 3(a),(d), and (g). For the noninteracting system, the fermions escape the cluster successively (i.e., starting at the edges, and finally from the center of the cluster). They move ballistically and the correlation function displays a fourfold symmetric structure, figures 3(b) and (c). In the interacting case, in contrast, the decay of a doublon into fermions is heavily suppressed. This results in a correlation function $\langle \hat{n}_i^s(t)\hat{n}_j^s(t)\rangle$ that has its main contributions within two square regions given by the light cones of fermions emitted by the outermost doublons of the cluster, see

figures 3(f) and (i). Within the light cones, single fermions are more likely to be found at lattice sites corresponding to a motion with almost maximal velocity $|v_{max}| = 2J$ into opposite direction. The density correlation between single fermions attains its largest values for nearest-neighbor lattice sites within the cloud, cf. figures 3(e),(f),(h), and (i). This may be due to virtual transitions between two configurations: either a doublon with a neighboring vacancy, or a state of two adjacent single fermions. Note that the mean total number of single fermions, $\sum_{i=1}^{L} \langle \hat{n}_i^s \rangle$, approaches within a few Jt an almost constant value, cf. area under the curves for $Jt = 3.5, 7.5$ and $U/J = 3, 6$ in the last column of figure 3. That means only the edges of the cluster evaporate for large interactions, releasing a finite number of single fermions. Moreover, $\langle \hat{n}_i^s(t) \rangle$ becomes relatively flat in the center of the cloud for larger evolution times Jt.

Let us now consider the spatial distribution of spin-entangled fermions during the expansion. For this purpose, the concurrence between two fermions at different lattice sites is numerically evaluated using equation (6). Figure 4 shows the concurrence for any pair of lattice sites i and j, at different times Jt and onsite interaction strengths U/J.

For the expansion of noninteracting fermions, figures 4(a)-(c), the concurrence is finite only for nearby lattice sites. It is almost 1 within the outermost wings of the expanding cloud. This can be physically understood the following way: Due to the Pauli principle, fermions with the same spin become spatially antibunched during the expansion. Thus, fermions at neighboring sites are more likely to have opposite spin, cf. figures 2(c)-(e). In addition, the outermost region of the cloud lies only within the light cones of the doublons close to the edge of the initial cluster. Two fermions detected in this region are almost certaitly emitted by the same edge doublon and in consequence have a high probability to be spin-entangled.

When increasing the onsite interaction U, spin-entangled pairs are formed on remote lattice sites, too, cf. figures 4(d)-(i). Indeed, spin-entanglement is found between lattice sites within and outside the initial cluster position, figures 4(e) and (h), as well as on different sides of the initial cluster position, figures 4(f) and (i).

The figures are a fingerprint of the creation of a counter propagating hole and single fermion by the decay of an edge doublon. When the hole moves through the cluster, the spin-entanglement with the single fermion outside the cluster is swapped sequentially from one fermion to the next in the cluster. In this way fermions become entangled that have never been on the same lattice site and have never directly interacted with each other. At the end of this process, a spin-singlet pair is created with a fermion at each side of the cluster. The concurrence for two fermions on different sides of the initial cluster position increases with the interaction strength, compare figures 4(f) and 4(i). This can be understood by the suppression of the decay probability of doublons with increasing interaction strengths. For larger interaction strength, a hole is more likely to cross the cluster without being disturbed by another hole.

For nearest-neighbor sites, which have a relatively large probability to be simultaneously singly occupied [see figures 3(f) and (i)], we observe a concurrence close to 1. This implies the creation of vacant lattice sites within the cloud during the expansion. The singlet pairs on nearest-neighbor sites come from virtual transitions between a doublon with neighboring vacancy and a state of two single fermions. We verified this behaviour in addition by numerically creating an ensemble of snapshots for the distribution of fermions as described in [19].

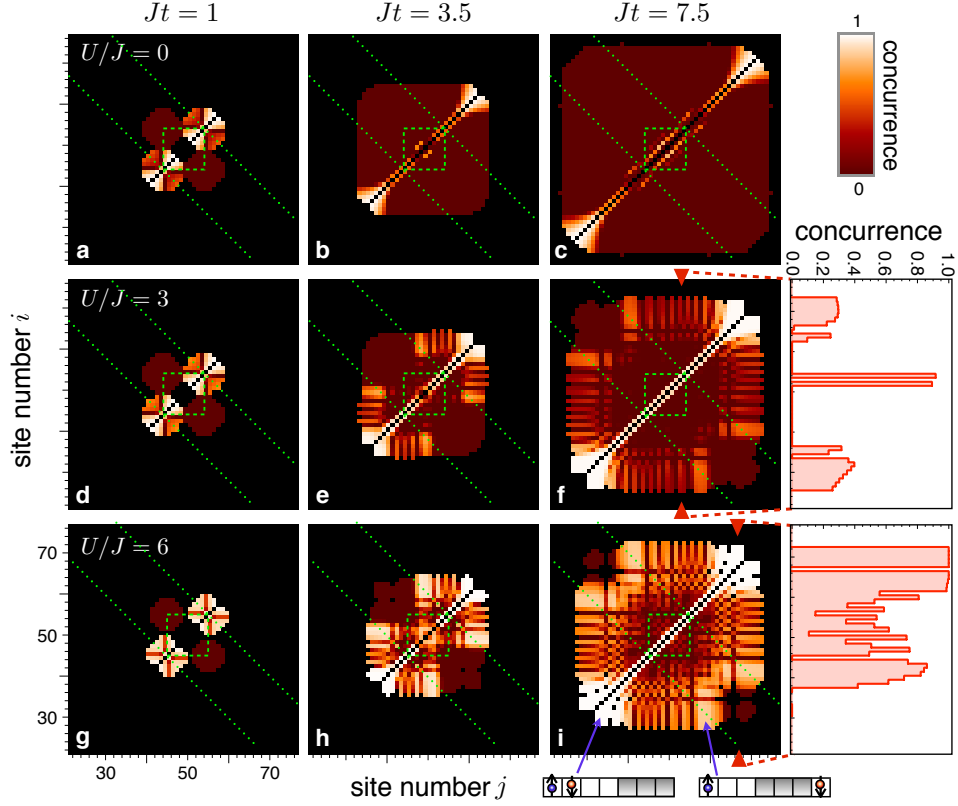We emphasize that for inhomogeneous systems, such as the one discussed in

Figure 4. Concurrence $C_{i,j}(t)$ of two (single) fermions located at lattices sites i and j after different expansion times Jt, see equation (6). Initially, ten doublons are located at the sites indicated by the dashed square. We emphasize that dark red indicates strictly zero concurrence (also see the cuts displayed to the right). The black colour code is used whenever the probability of finding fermions at sites i and j is too small, $\langle \hat{n}_i^s(t)\hat{n}_j^s(t)\rangle < 10^{-5}$. In those cases, the concurrence is not computed as it would become susceptible to numerical inaccuracies. (a,d,g) For short evolution times, here $Jt = 1$, single fermions are mainly created at the edge of the cluster since the central fermions are initially Pauli blocked. Fermions close to the same edge of the cloud are likely to be entangled as they are likely to originate from the same doublon. Fermions at opposite edges are not entangled since they can not have been emitted from the same doublon. (b,c) At larger evolution times and without onsite interactions, the concurrence is 0 for most sites i and j. However, it is close to 1 when two fermions are located at the outermost part of the cloud. (e,f,h,i) By increasing the onsite interaction U/J, entanglement of fermions across the cluster becomes possible. In this case, the concurrence is highest when the fermions result from the decay of a doublon at the edge and escape with opposite velocity, indicated by the dotted line [see also cut through panel (i)]. Moreover, the concurrence of fermions at neighboring sites becomes almost 1. Within the central region, approximately given by the overlap of the light cones shown in figure 1, the concurrence remains relatively small.
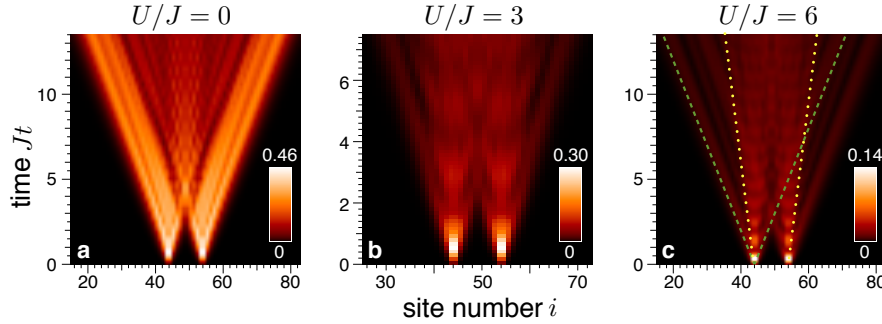
Figure 5. Spin-entanglement of a single lattice site i with all the other sites. The panels show the time evolution of $C_{tot,i}(t)$, given by equation (8), for different interaction strengths U/J. (a) In the absence of interaction, it is primarily the sites at the edge of the cloud which are spin-entangled. (b,c) For finite interactions, we observe the following: At larger times $C_{tot,i}(t)$ is nearly homogeneous in a central region within the doublon light cones [dotted lines in (c)]. Spin-entanglement for lattice sites removed from this central region is finite at locations corresponding to trajectories of fermions, which have dissolved from the edges of the cluster. For the left edge the single fermion light cone is shown as dashed lines.

this article, the spatially resolved measurement of two-point correlations provides more information about the dynamics than structure factors, such as $S_k \propto \sum_{lm} e^{-ik(l-m)} \langle \hat{S}_l^z \hat{S}_m^z \rangle$. While the latter could be used to determine the average spin-spin correlation of fermions at fixed distance, it contains no information where these spin-correlated pairs are located in the cloud.

3.3. Summed concurrences

Above, we examined the spin-entanglement between two lattice sites for fixed time points. In this subsection we aim to quantify the spin-entanglement for entire regions in the lattice. In particular, we address the questions: Are there sites which share more spin-entanglement with the rest than other lattice sites? How does the spin-entanglement in different regions built up as function of time? Which locations are most entangled in the weakly and strongly interacting case? How does the size of the cluster affect these results?

In the following we discuss the amount of pairwise spin-entanglement of a lattice site or a region in the lattice in terms of the *summed concurrence*. We define it as the sum over the concurrences, $C_{i,j}(t)$, which are weighted by the probability of detecting a single fermion at both lattice sites, $\langle \hat{n}_i^s(t) \hat{n}_j^s(t) \rangle$. The weights are introduced to accommodate for the possibility of vacant or doubly occupied lattice sites, in contrast to the summed concurrence used in spin systems [45]. For a system consisting of spin-singlet pairs whose wavefunctions do not overlap, i.e., $C_{i,j}(t)$ is either zero or one for all sites i and j, the summed concurrence equals the average number of delocalized spin-singlet pairs. Note that the summed concurrence is by no means a measure for the total entanglement of the system. It neither includes multipartite entanglement nor entanglement in the occupation numbers. For a detailed discussion on entanglement in many-body systems we refer to [46], see also [47, 48, 49, 16] for recent proposals on detecting entanglement in cold atom systems.

Let us consider the spin-entanglement of a site with all the other lattice sites.

The summed concurrence for site i is defined by

$$C_{tot,i}(t) = \sum_{j \neq i} \langle \hat{n}_i^s(t) \hat{n}_j^s(t) \rangle \, C_{i,j}(t). \tag{8}$$

The time evolution of $C_{tot,i}(t)$ is shown in figure 5 for different interaction strengths U/J. For noninteracting fermions [figure 5(a)], lattice sites close to the edge of the cloud display the strongest entanglement, while sites in the rest of the cloud are hardly entangled. For increasing interaction strengths a central region with almost uniform $C_{tot,i}(t)$ builds up during the evolution, see figures 5(b) and (c). For large U/J, we find that $C_{tot,i}(t)$ approaches the expectation value $\langle \hat{n}_i^s \rangle$. This turns out to be related to the fact that in this case the probability of having two doublons decay is negligible, and the contribution comes almost entirely from the decay of a single doublon.

In figure 4(i) it is apparent that onsite interactions can lead to spin entanglement across the expanding cluster. In the following we compare the summed concurrences of lattice sites on the same side and on different sides of the initial cluster location, C_{ss} and C_{ds}, respectively. They are defined by

$$C_{ss}(t) = \sum_{i+1 < j < l \, \vee \, i-1 > j > r} \langle \hat{n}_i^s(t) \hat{n}_j^s(t) \rangle \, C_{i,j}(t) \tag{9}$$

$$C_{ds}(t) = \sum_{i < l \, \wedge \, j > r} \langle \hat{n}_i^s(t) \hat{n}_j^s(t) \rangle \, C_{i,j}(t), \tag{10}$$

where l and r denote the leftmost and rightmost occupied lattice sites of the initial state. Note that nearest-neighbor lattice sites are excluded from $C_{ss}(t)$. That means we do not take into account contributions from virtual transitions of doublons (decaying virtually into two adjacent fermions) that move away from the cluster initial position. In addition, we consider the summed concurrence of sites at fixed distance d, $C_d(t) = \sum_i \langle \hat{n}_i^s(t) \hat{n}_{i+d}^s(t) \rangle C_{i,i+d}(t)$, and the summed concurrence of all sites, $C_{tot}(t) = \sum_{i<j} \langle \hat{n}_i^s(t) \hat{n}_j^s(t) \rangle C_{i,j}(t)$. The time evolution of these summed concurrences is shown in figure 6.

For *noninteracting* fermions and small evolution times, the total summed concurrence is dominated by contributions from nearest-neighbor sites. For larger times more and more spin-entanglement is transferred to fermions found on the same side of the initial cluster position (C_{ss}), see figure 6(a). The spin-entanglement remains relevant only for small distances, reflected in $C_8(t) = 0$ for all simulated times, cf. figure 6(d).

By contrast, in the *interacting* case, spin-entanglement is generated via fermions propagating away on different sides of the cluster. This is seen as a finite value of $C_{ds}(t)$ for times $Jt \gtrsim 5$, which is the time a hole needs to propagate through the cluster, cf. figures 6(b) and (c). The total summed concurrence and concurrence between nearest-neighbor sites quickly settle into a damped oscillation around a constant value. The time evolution of the summed concurrence of sites at distance $d \geq 2$ is displayed in figures 6(e) and (f). $C_d(t)$ remains zero for small times, peaks at times Jt slightly exceeding $d/4$, and decreases for larger times. This shows that spin-entangled pairs mainly propagate at almost maximal (relative) velocity $4J$. For large U/J, $C_d(t)$ is approximately uniform for distances $d \leq 4Jt$ and roughly decays as $(Jt)^{-1}$ for the simulated times. Note that $C_1(t)$ plays a special role. Its main contribution does not stem from "free" fermions. Rather, it is generated by a doublon virtually dissolving into adjacent fermions.
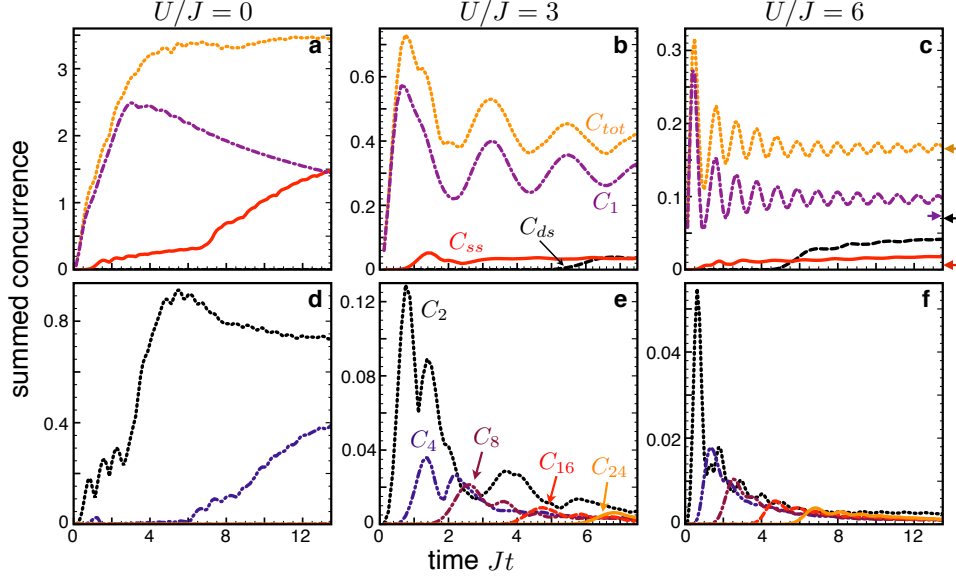
Figure 6. Time evolution of spin-entanglement in different areas of the expanding cloud. (a-c) We show: the summed concurrence C_{tot} of all lattice sites, the summed concurrence C_1 between nearest-neighbor sites, as well as the summed concurrences of all lattice sites at same side (C_{ss}) and at different sides (C_{ds}) of the cloud (see the main text for the definitions). Nonvanishing C_{ds} is found only for finite onsite interaction. C_{tot} and C_1 quickly settle into a damped oscillation around a constant value, for $U/J \gtrsim 2$. The arrows in panel (c) show corresponding values of the summed concurrences for the decay of a single doublon, cf. figure 7. (d-f) Summed concurrence C_d of lattice sites at distance $d \geq 2$. (d) Without interactions only close lattice sites are spin-entangled. (e,f) With increasing interaction strength U/J, $C_d(t)$ equals zero for times up to $Jt \approx d/4$, followed by a peak and a decay for larger times. At fixed time C_d is approximately uniform for the distances $d \lesssim 4Jt$.

Let us finally discuss the impact of the cluster size on the spin-entanglement dynamics. For very weak interactions, a larger number of doublons means that more delocalized singlet pairs are created shortly after switching off the confining potential. For large interaction strengths up to $U/J = 40$, we simulate the expansion and compare the summed concurrences for different cluster sizes, including the case of a single doublon. We summarize the results in figure 7. Note that reasonably large evolution times ($Jt \approx 20$) for the comparison of the summed concurrences are reached only for $U/J \gtrsim 6$. The summed concurrence of all sites, C_{tot}, agrees for all considered cluster sizes and matches the analytical result for a single doublon, see figure 7(a). Apparently, the initially Pauli-blocked core has no effect on the number of created single fermions for the considered times. For C_{ss} and C_{ds}, however, we find a clearly different behaviour for a single doublon and a cluster of four and more doublons [figure 7(b)]: A cluster is more likely to emit (delocalized) spin-entangled pairs into the same direction.
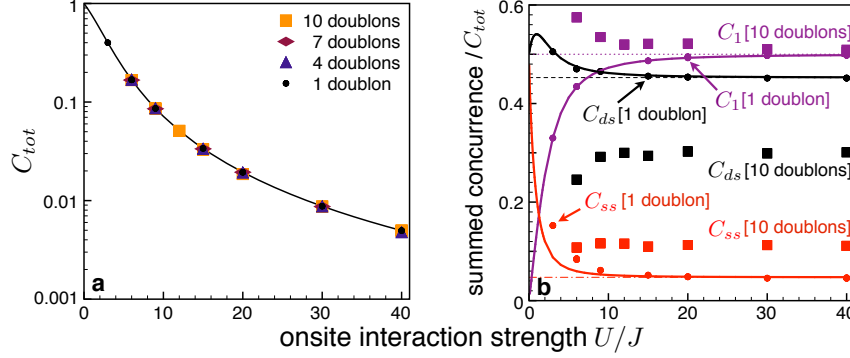
Figure 7. Summed concurrences for different sizes of the initial cluster. We compute the values at time $Jt = 20$ (except for $U/J = 6$, where $Jt = 13.5$), when they are almost constant as function of time. (a) The total summed concurrence, C_{tot}, shows no dependence on the cluster size for large onsite interaction strengths $U/J \geq 6$. The data agrees with the exact result for a single doublon derived in appendix C, $C_{tot} = 1 - [1 + 16J^2/U^2]^{-1/2}$, which is shown as solid line. (b) The summed concurrences of lattice sites at same side (C_{ss}) and at different sides (C_{ds}) of the cloud (see the main text for the definitions) disagrees for a single doublon (dots) and a cluster of doublons (squares). Note that clusters of sizes 4,7, and 10 give similar values. For strong interactions, a cluster prefers the emission of (delocalized) singlet pairs into the same direction compared to a single doublon. The summed concurrence between nearest-neighbor sites (C_1) approaches $C_{tot}/2$ in both cases. Solid lines show analytical results for C_1 as well as the contribution of scattering states to C_{ss} and C_{ds} for a single doublon (see appendix C).

3.4. Expansion with modulated tunneling amplitude

In the previous section we have seen for the interacting case that total summed concurrence, C_{tot}, approaches a fixed value shortly after switching off the potential, via the escape of a few fermions from the cluster edges. Here, we discuss a way of "continuously " generating single fermions and enhancing C_{tot} compared to the free time evolution. We consider an expansion during which the tunneling amplitude is repeatedly varied in time, while the interaction strength is constant. Such modulation may be experimentally realized by either varying the laser intensity (the tunneling amplitude decreases much faster with increased laser intensity than the onsite interaction strength, see, e.g., [1]) or by shaking the lattice sinusoidally [50]. We find for certain values of the tunneling amplitudes and time intervals between the quenches an increased amount of spin-entanglement as shown in figure 8. For the presented case, the repeated quenches lead to the generation of more and more single fermions, see figure 8(a). This results in an enhanced spin-entanglement between distant lattice sites, while the spin-entanglement between nearest-neighbor sites is suppressed [compare figures 8(b) and 8(c) with figures 6(c) and 6(f)].

4. Remarks on observing the spin-entanglement in experiments

In the main part of this article we have analyzed the dynamics of the spin-entanglement for the expansion from a cluster of doublons. As discussed in section 3.1 the concurrence between two lattice sites i and j can be determined by the single fermion expectation value $\langle \hat{n}_i^s(t) \hat{n}_j^s(t) \rangle$ and the spin-spin correlation $\langle \hat{S}_i^z(t) \hat{S}_j^z(t) \rangle =$
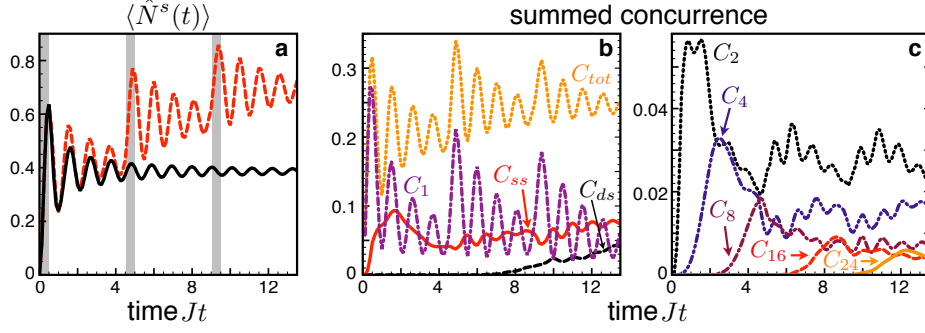
Figure 8. Expansion with time-dependent tunneling amplitude (modulated in a stepwise fashion). The tunneling amplitude is repeatedly switched between the values J [time intervals marked by gray background in panel (a)] and $J' = J/2$ [white background in panel (a)], while the onsite interaction strength is fixed at $U/J = 6$. (a) This dynamics (dashed line) produces a larger total number of single fermions $\langle \hat{N}^s(t) \rangle$ than the free expansion with amplitude J (solid line). (b,c) Time evolution of the summed concurrences. In comparison to the free expansion, cf. figures 6(c) and (f), the total summed concurrence as well as the concurrences C_{ss} and C_{ds} are enhanced, while the summed concurrence at nearest-neighbor sites, C_1, is decreased. This is also seen in the enlarged summed concurrence of sites at distances $d \geq 2$.

$\frac{1}{4}\langle [\hat{n}_{i,\uparrow}(t) - \hat{n}_{i,\downarrow}(t)][\hat{n}_{j,\uparrow}(t) - \hat{n}_{j,\downarrow}(t)] \rangle$.

Experimentally, both expectation values could be obtained by averaging over many snapshots of the spin-dependent single-site fermionic particle number analogous to the already implemented single-site detection of bosonic particles [11, 12]. Since doubly occupied lattice sites do not contribute to these expectation values, it would suffice to be able to detect singly occupied sites. Thus, the loss of atom pairs due to inelastic light-induced collision during the imaging process, showing up in the bosonic case, would not be an issue.

Measuring correlations of the spin-z component will be sufficient for obtaining the concurrence under the following assumptions: (i) the initial state is of the type we have described (total singlet, i.e. total spin 0); (ii) the dynamics proceeds according to the model Hamiltonian, i.e., a SU(2) symmetric Hamiltonian with no decoherence or entanglement with external degrees of freedom. A scenario where the initial state violates condition (i) would be a cluster with impurity sites that contain only single fermions. If there is only one impurity containing a single fermion, then the problem can still be diagnosed because the final snapshot will reveal unequal numbers of spin-up and spin-down fermions. In general, however, if these two conditions are in doubt, the experiment would have to measure the full spin-spin density matrix of two lattice sites, by repeated runs and measurements of spin projections in different directions. This could be done by implementing a rotation in spin space before measurements, in analogy to the state tomography realized with trapped ions [51]. While being more challenging than measuring the spin-dependent fermion number, such a kind of coherent spin control seems to be possible in future experiments. Spin flips at single lattice sites have already been shown experimentally for ultracold bosons [52]. This setup could be in principle extended to coherent spin control, replacing the Rabi frequency sweep by driving a Rabi oscillation [53].

5. Summary and Outlook

In this article, we have analyzed the creation and time-evolution of spin-entanglement during the sudden expansion from a cluster of doublons into an empty lattice. Interestingly, remote spin-entangled pairs are created for large onsite interaction. In addition, an extended cluster favours the emission of the two fermions of a pair into the same direction when compared against the decay of a single doublon. Finally, we found that a time-dependent modulation of the tunneling amplitude can be used to increase the "production" of spin-entangled pairs. Our results provide a starting point for studying the spin-entanglement dynamics for more complex initial states or, e.g., for spin-imbalanced fermionic gases.

In the scenario considered here, the spin-entanglement can be extracted from the two-site spin-z correlation functions. Thus, it will become experimentally accessible once spin-dependent single-site detection has been implemented.

Appendix A. Correlation functions and concurrence of noninteracting fermions

In this appendix, we derive analytical formulae for the correlation functions of expanding, *noninteracting* fermions. For vanishing onsite interaction, fermions of different species are uncorrelated and each fermion propagates with the free dispersion. The time evolution of the annihilation operators is given by

$$\hat{c}_{j,a}(t) = \sum_m G_{jm}(t)\hat{c}_{m,a}, \tag{A.1}$$

with spin index $a = \uparrow, \downarrow$ and the free fermion propagator

$$G_{jm}(t) = \int_{-\pi}^{\pi} \frac{\mathrm{d}k}{2\pi} \exp\{i[(m-j)k - 2J\cos(k)t]\} = i^{j-m}\mathcal{J}_{j-m}(2Jt). \tag{A.2}$$

Here, $\mathcal{J}$ denotes the Bessel function of the first kind and we assumed an infinite lattice. For the previously discussed initial state of localized doublons, the Green's function reads

$$\mathcal{G}_{ij}(t) = \langle \hat{c}_{i,a}^{\dagger}(t)\hat{c}_{j,a}(t) \rangle = i^{j-i} \sum_{m \in O} \mathcal{J}_{j-m}(2Jt)\mathcal{J}_{i-m}(2Jt), \tag{A.3}$$

where the summation is taken over all initially occupied lattice sites O. For both spin species, the density is given by

$$\mathcal{N}_i(t) = \mathcal{G}_{ii}(t) = \sum_{m \in O} \mathcal{J}_{|i-m|}^2(2Jt). \tag{A.4}$$

When the fermions are initially localized at the lattice sites, equal time, normal ordered products of operators can be expressed as a Slater determinant of the equal time one-particle Green's functions, $\mathcal{G}_{ij}(t)$, [54]. The correlation function $\langle \hat{S}_i^z(t)\hat{S}_j^z(t) \rangle$ can be evaluated by writing it in terms of density-density correlations and making use

of $\langle \hat{n}_{i,a}(t)\hat{n}_{j\neq i,b}(t)\rangle = \mathcal{N}_i(t)\mathcal{N}_j(t) - \delta_{ab}\left|\mathcal{G}_{ij}(t)\right|^2$ and $\langle \hat{n}_{i,a}(t)\hat{n}_{i,b}(t)\rangle = \mathcal{N}_i^{(2-\delta_{ab})}$. This yields

$$\langle \hat{S}_i^z(t)\hat{S}_{j\neq i}^z(t)\rangle = -\frac{1}{2}\left|\mathcal{G}_{ij}(t)\right|^2, \tag{A.5}$$

$$\langle \hat{S}_i^z(t)\hat{S}_i^z(t)\rangle = \frac{1}{2}\mathcal{N}_i(t)\left[1-\mathcal{N}_i(t)\right]. \tag{A.6}$$

Note that the probability of finding two fermions with the same spin at lattice sites i and j is by $2|\mathcal{G}_{ij}(t)|^2$ smaller than the probability for fermions with antiparallel spin. This difference leads to a nonvanishing spin-spin correlation even in the absence of onsite interactions. For noninteracting fermions, the spin-spin correlation is related to the density-density correlation $D_{ij}(t) = \langle \hat{n}_i(t)\hat{n}_j(t)\rangle - \langle \hat{n}_i(t)\rangle\langle \hat{n}_j(t)\rangle$ via

$$D_{ij}(t) = 4\langle \hat{S}_i^z(t)\hat{S}_j^z(t)\rangle. \tag{A.7}$$

Thus, the density-density correlation $D_{ij}(t)$ is smaller or equal to zero for different lattice sites i and j, cf. figures 2(a) and (c)-(e). Analogously, the density-density correlation of single fermions is calculated using the relations for $\langle \hat{n}_{i,a}(t)\hat{n}_{j,b}(t)\rangle$ given above. We find

$$\langle \hat{n}_i^s(t)\hat{n}_i^s(t)\rangle = 2\mathcal{N}_i(t)\left[1-\mathcal{N}_i(t)\right], \tag{A.8}$$

$$\langle \hat{n}_i^s(t)\hat{n}_{j\neq i}^s(t)\rangle = 4\left[N_i(t) - \left(\mathcal{N}_i(t)\mathcal{N}_j(t) - |\mathcal{G}_{ij}(t)|^2\right)\right] \times \tag{A.9}$$
$$\left[N_j(t) - \left(\mathcal{N}_i(t)\mathcal{N}_j(t) - |\mathcal{G}_{ij}(t)|^2\right)\right] - 2\left|\mathcal{G}_{ij}(t)\right|^2.$$

The concurrence $C_{i,j}(t)$ [defined by equation (6)] can be evaluated using the expressions (A.5) and (A.9). It approaches one in the limit $\langle \hat{S}_i^z(t)\hat{S}_{j\neq i}^z(t)\rangle/\langle \hat{n}_i^s(t)\hat{n}_{j\neq i}^s(t)\rangle \searrow -\frac{1}{4}$. This is the case for $|\mathcal{G}_{ij\neq i}(t)|^2 \nearrow \mathcal{N}_i(t)\mathcal{N}_{j\neq i}(t)$ (note that $|\mathcal{G}_{ij\neq i}(t)|^2$ can only assume values between 0 and 1/2).

Appendix B. Decay of a doublon into scattering states

This appendix presents the derivation of the decay probability of a fermionic doublon into different scattering states $|\psi_{K,k}\rangle$. In doing so, the wavefunctions of the scattering states are calculated mainly adopting the procedure for two-particle states in the Bose Hubbard model presented in [55].

For one spin-up and one spin-down fermion, and an infinite lattice the Hamiltonian (1) can be expressed in the form

$$\hat{\mathcal{H}}_D = -J\sum_i \left\{|\uparrow_i\rangle\langle\uparrow_{i+1}| + |\uparrow_{i+1}\rangle\langle\uparrow_i| + |\downarrow_i\rangle\langle\downarrow_{i+1}| + |\downarrow_{i+1}\rangle\langle\downarrow_i|\right\}$$
$$+ U\sum_i |\uparrow_i,\downarrow_i\rangle\langle\uparrow_i,\downarrow_i|. \tag{B.1}$$

Analogously, we write the two-fermion states in terms of the basis $\{|\uparrow_i,\downarrow_j\rangle\}$, $|\Psi\rangle = \sum_{i,j}\Psi(\uparrow_i,\downarrow_j)|\uparrow_i,\downarrow_j\rangle$. For the decay of a doublon, the fermions are always in the spin-singlet subspace. Thus, we can write the two-particle wavefunction as $\Psi(\uparrow_i,\downarrow_j) = \varphi_s(\uparrow,\downarrow)\cdot\psi(i,j)$, with the spin-singlet wavefunction $\varphi_s(a,b) = \delta_{a,\uparrow}\delta_{b,\downarrow} - \delta_{a,\downarrow}\delta_{b,\uparrow}$ and a symmetric spatial wavefunction, $\psi(i,j) = \psi(j,i)$. Plugging $|\Psi\rangle$ into the Schrödinger equation for Hamiltonian (B.1) yields

$$(E - U\delta_{ij})\psi(i,j) = -J\left[\psi(i-1,j) + \psi(i+1,j) + \psi(i,j-1)\right.$$
$$\left.+\psi(i,j+1)\right]. \tag{B.2}$$

This relation is simplified by introducing center of mass (c.o.m.) and relative coordinates, $R = (i + j)/2$ and $r = i - j$, respectively. The wavefunction factorizes into a plane wave motion of the c.o.m. with total wavenumber $K \in [-\pi, \pi)$ and a K-dependent relative motion, i.e., $\psi(i, j) = e^{iKR}\psi_K(r)$. The relative motion satisfies the recurrence relation

$$- J_K \left[\psi_K(r - 1) + \psi_K(r + 1)\right] = \left(E_K - U\delta_{r0}\right)\psi_K(r), \qquad (B.3)$$

with K-dependent tunneling amplitude $J_K = 2J\cos(K/2)$ and energy E_K. For vanishing interaction strength U equation (B.3) is solved by plane waves $\psi_{K,k}(r) = e^{\pm ikr}$ with corresponding eigenenergies $E_{K,k} = -2J_K\cos(k)$. In the interacting case, we make a scattering ansatz by writing the wavefunction as a superposition of incoming and reflected plane waves, $\psi_{K,k}(r \geq 0) = e^{ikr} + c\,e^{-ikr}$. Here, k is the relative wavenumber and $\psi_{K,k}(r < 0)$ is determined by the symmetry condition $\psi(r) = \psi(-r)$. The boundary condition at $r = 0$ in equation (B.3) fixes the coefficient c and we obtain

$$\psi_{K,k}(r) = \psi_{K,k}(0)\left[\cos(kr) + \frac{U}{2J_K\sin(k)}\sin(k|r|)\right]. \qquad (B.4)$$

Finally, we compare the decay probability of a doublon for different scattering states $|\psi_{K,k}\rangle$. In doing so, we express $|\psi_{K,k}(0)|^2$ in terms of the average density in the relative coordinate, $\bar{n}$, which is obtained by averaging $|\psi_{K,k}(r)|^2$ over one period $2\pi/k$. Note that $\bar{n}$ does only depend on the systems size and is independent of k, K, and U. We find that the decay probability into the scattering state $|\psi_{K,k}\rangle$ equals

$$|\psi_{K,k}(0)|^2 = \bar{n}\left[1 + U^2/\left(16J^2\cos^2(K/2)\sin^2(k)\right)\right]^{-1}. \qquad (B.5)$$

Appendix C. Summed concurrences of a single doublon

This appendix provides the calculation of the summed concurrences for the expansion from a single doublon. The results are depicted in figure 7. For this initial state, the fermions form a spin-singlet for all times. Consequently, the concurrence $C_{i,j}(t)$ [defined by equation (6)] equals one for all sites i and j, and the summed concurrences simplify to sums over the expectation values $\langle \hat{n}_i^s(t)\hat{n}_j^s(t)\rangle$, see section 3.3.

Let us first consider the total summed concurrence for a single doublon $C_{tot}(t) = \sum_{i<j}\langle \hat{n}_i^s(t)\hat{n}_j^s(t)\rangle$. This is nothing but the probability of finding the fermions at different lattice sites. It can be expressed as $1 - P_D(t)$, with the doublon survival probability $P_D(t)$, i.e., the probability of finding the doublon intact at time t. In the long time limit, only fermions in a bound state remain localized close to each other. For a singlet pair with finite onsite interaction $U \neq 0$ and c.o.m. wavenumber K, it exists one bound state $\psi_K^b(r)$ [localized solution of equation (B.3), details are given below], where r is the relative coordinate. Thus, we obtain $P_D(\infty) = \frac{1}{2\pi}\int_{-\pi}^{\pi}dK\,|\psi_K^b(0)|^4$ in the limit of an infinite lattice, where $\psi_K^b(0)$ is the overlap between the doublon and the bound state. Analogously, we find $C_1(\infty) = \frac{1}{2\pi}\int_{-\pi}^{\pi}dK\,|\psi_K^b(0)|^2|\psi_K^b(1)|^2$, where we have used that $C_1(t) = \sum_i\langle \hat{n}_i^s(t)\hat{n}_{i+1}^s(t)\rangle$ equals the probability of finding the fermions at time t at nearest-neighbor lattice sites. The bound state can be calculated using the exponential ansatz $\psi_K^b(r) = 1/\sqrt{\mathcal{N}_K}\cdot\alpha_K^{|r|}$ for the wavefunction in equation (B.3). This gives $\alpha_K = U/2J_K - \text{sign}(U/2J_K)\cdot\sqrt{1 + (U/2J_K)^2}$ and $\mathcal{N}_K = (2J_K/U)\cdot\sqrt{1 + (U/2J_K)^2}$, with $J_K = 2\cos(K/2)$. Inserting this solution into the doublon survival probability yields $P_D(\infty) = \frac{1}{2\pi}\int_{-\pi}^{\pi}dK\,\mathcal{N}_K^{-2} = [1 + 16J^2/U^2]^{-1/2}$.

In the limit of infinite times, the total summed concurrence and summed concurrence of nearest-neighbor lattice sites are, hence, given by

$$C_{tot}(\infty) = 1 - [1 + 16J^2/U^2]^{-1/2} = 8J^2/U^2 + \mathcal{O}([J/U]^4), \qquad \text{(C.1)}$$

$$C_1(\infty) \;\; = \frac{1}{2\pi} \int_{-\pi}^{\pi} \mathrm{d}K \, |\alpha_K|^2 \mathcal{N}_K^{-2} = 4J^2/U^2 + \mathcal{O}([J/U]^4). \qquad \text{(C.2)}$$

In the long-time limit, the summed concurrences of lattice sites at same side $(C_{ss}(t))$ and at different sides $(C_{ds}(t))$ of initial doublon position can be related to the scattering states calculated in appendix B. We denote by $C_{ds}^{(scat)}$ and $C_{ss}^{(scat)}$ the contributions to the summed concurrences stemming from the scattering states. $C_{ds}^{(scat)}$ is the sum of the occupation probabilities of scattering states corresponding to fermions moving in opposite direction [$k_1 \in (0, \pi)$, $k_2 \in (-\pi, 0)$ or $k_1 \in (-\pi, 0)$, $k_2 \in (0, \pi)$], and $C_{ss}^{(scat)}$ is the sum of the occupation probabilities of those states with fermions moving into the same direction [$k_1, k_2 \in (0, \pi)$ or $k_1, k_2 \in (-\pi, 0)$]. Here, k_1 and k_2 denote the asymptotic wavenumbers of the two fermions. The occupation probabilities are the absolute square of the overlap between the doublon and the scattering state, $|\psi_{K,k}(0)|^2$. The explicit form of $|\psi_{K,k}(0)|^2$ is given by equation (B.5). Taking the continuum limit we find

$$C_{ds}^{(scat)} = \frac{1}{(2\pi)^2} \left[\int_0^\pi \mathrm{d}k_1 \int_{-\pi}^0 \mathrm{d}k_2 + \int_{-\pi}^0 \mathrm{d}k_1 \int_0^\pi \mathrm{d}k_2 \right] \qquad \text{(C.3)}$$

$$\times \left[1 + U^2 / \left(16J^2 \cos^2([k_1 + k_2]/2) \sin^2([k_1 - k_2]/2) \right) \right]^{-1}$$

$$= 4\frac{J^2}{U^2}[1/2 + 4/\pi^2] + \mathcal{O}([J/U]^4), \qquad \text{(C.4)}$$

$$C_{ss}^{(scat)} = \frac{1}{(2\pi)^2} \left[\int_0^\pi \mathrm{d}k_1 \int_0^\pi \mathrm{d}k_2 + \int_{-\pi}^0 \mathrm{d}k_1 \int_{-\pi}^0 \mathrm{d}k_2 \right] \qquad \text{(C.5)}$$

$$\times \left[1 + U^2 / \left(16J^2 \cos^2([k_1 + k_2]/2) \sin^2([k_1 - k_2]/2) \right) \right]^{-1}$$

$$= 4\frac{J^2}{U^2}[1/2 - 4/\pi^2] + \mathcal{O}([J/U]^4). \qquad \text{(C.6)}$$

The summed concurrences $C_{ss}(t)$ and $C_{ds}(t)$ used for the numerical data [equations (9) and (10)] contain additional contributions from bound states. In the definition of $C_{ss}(t)$ we excluded nearest-neighbor lattice sites in order to remove most of these contributions [note that nearest-neighbor sites do not appear in $C_{ds}(t)$]. From the expression for the bound state given above follows that all other terms are of the order $\mathcal{O}([J/U]^4)$. Thus, $C_{ss}(t)$ and $C_{ds}(t)$ agree with $C_{ss}^{(scat)}$ and $C_{ds}^{(scat)}$ for large Jt and U/J, cf. figure 7(b).

In conclusion, we find following relations between the summed concurrences for long evolution times and large interaction strengths $U/J \gg 1$: $C_1 = C_{tot}/2$, $C_{ss} = [1/4 - 2/\pi^2]C_{tot}$, and $C_{ds} = [1/4 + 2/\pi^2]C_{tot}$.

References

[1] Bloch I, Dalibard J and Zwerger W 2008 Many-body physics with ultracold gases *Rev. Mod. Phys.* **80** 885–964

[2] Polkovnikov A, Sengupta K, Silva A and Vengalattore M 2011 Nonequilibrium dynamics of closed interacting quantum systems *Rev. Mod. Phys.* **83** 863–883

[3] Greiner M, Mandel O, Hänsch T W and Bloch I 2002 Collapse and revival of the matter wave field of a Bose-Einstein condensate *Nature* **419** 51

[4] Widera A, Trotzky S, Cheinet P, Fölling S, Gerbier F, Bloch I, Gritsev V, Lukin M D and Demler E 2008 Quantum Spin Dynamics of Mode-Squeezed Luttinger Liquids in Two-Component Atomic Gases *Phys. Rev. Lett.* **100** 140401

[5] Chen D, White M, Borries C and DeMarco B 2011 Quantum Quench of an Atomic Mott Insulator *Phys. Rev. Lett.* **106** 235304

[6] Schneider U, Hackermüller L, Ronzheimer J P, Will S, Braun S, Best T, Bloch I, Demler E, Mandt S, Rasch D and Rosch A 2012 Fermionic transport and out-of-equilibrium dynamics in a homogeneous Hubbard model with ultracold atoms *Nature physics* **8** 213

[7] Ott H, de Mirandes E, Ferlaino F, Roati G, Modugno G and Inguscio M 2004 Collisionally Induced Transport in Periodic Potentials *Phys. Rev. Lett.* **92** 160601

[8] Pezzè L, Pitaevskii L, Smerzi A, Stringari S, Modugno G, de Mirandes E, Ferlaino F, Ott H, Roati G and Inguscio M 2004 Insulating Behavior of a Trapped Ideal Fermi Gas *Phys. Rev. Lett.* **93** 120401

[9] Strohmaier N, Takasu Y, Günter K, Jördens R, Köhl M, Moritz H and Esslinger T 2007 Interaction-Controlled Transport of an Ultracold Fermi Gas *Phys. Rev. Lett.* **99** 220601

[10] Würtz P, Langen T, Gericke T, Koglbauer A and Ott H 2009 Experimental Demonstration of Single-Site Addressability in a Two-Dimensional Optical Lattice *Phys. Rev. Lett.* **103** 080404

[11] Bakr W S, Gillen J I, Peng A, Fölling S and Greiner M 2009 A quantum gas microscope for detecting single atoms in a Hubbard-regime optical lattice *Nature* **462** 74

[12] Sherson J F, Weitenberg C, Endres M, Cheneau M, Bloch I and Kuhr S 2010 Single-atom-resolved fluorescence imaging of an atomic Mott insulator *Nature* **467** 68

[13] Cheneau M, Barmettler P, Poletti D, Endres M, Schauß P, Fukuhara T, Gross C, Bloch I, Kollath C and Kuhr S 2012 Light-cone-like spreading of correlations in a quantum many-body system *Nature* **481** 484

[14] Barmettler P, Poletti D, Cheneau M and Kollath C 2012 Propagation front of correlations in an interacting bose gas *Phys. Rev. A* **85** 053625

[15] Fukuhara T, Kantian A, Endres M, Cheneau M, Schauß P, Hild S, Bellem D, Schollwöck U, Giamarchi T, Gross C, Bloch I and Kuhr S 2012 Quantum dynamics of a single, mobile spin impurity *arXiv:1209.6468*

[16] Daley A J, Pichler H, Schachenmayer J and Zoller P 2012 Measuring Entanglement Growth in Quench Dynamics of Bosons in an Optical Lattice *Phys. Rev. Lett.* **109** 020505

[17] Barmettler P and Kollath C 2011 Controllable manipulation and detection of local densities and bipartite entanglement in a quantum gas by a dissipative defect *Phys. Rev. A* **84** 041606(R)

[18] Gammelmark S and Mølmer K 2010 Simulating local measurements on a quantum many-body system with stochastic matrix product states *Phys. Rev. A* **81** 012120

[19] Keßler S, Holzner A, McCulloch I P, von Delft J and Marquardt F 2012 Stroboscopic observation of quantum many-body dynamics *Phys. Rev. A* **85** 011605(R)

[20] Kajala J, Massel F and Törmä P 2011 Expansion dynamics in the One-Dimensional Fermi-Hubbard Model *Phys. Rev. Lett.* **106** 206401

[21] Langer S, Schuetz M J A, McCulloch I P, Schollwöck U and Heidrich-Meisner F 2012 Expansion velocity of a one-dimensional, two-component fermi gas during the sudden expansion in the ballistic regime *Phys. Rev. A* **85** 043618

[22] Heidrich-Meisner F, Rigol M, Muramatsu A, Feiguin A E and Dagotto E 2008 Ground-state reference systems for expanding correlated fermions in one dimension *Phys. Rev. A* **78** 013620

[23] Karlsson D, Verdozzi C, Odashima M M and Capelle K 2011 Dynamical self-stabilization of the Mott insulator: Time evolution of the density and entanglement entropy of out-of-equilibrium cold fermion gases *EPL* **93** 23003

[24] Mandt S, Rapp A and Rosch A 2011 Interacting Fermionic Atoms in Optical Lattices Diffuse Symmetrically Upwards and Downwards in a Gravitational Potential *Phys. Rev. Lett.* **106** 250602

[25] Kajala J, Massel F and Törmä P 2011 Expansion dynamics of the Fulde-Ferrell-Larkin-Ovchinnikov state *Phys. Rev. A* **84** 041601

[26] Lu H, Baksmaty L O, Bolech C J and Pu H 2012 Expansion of 1D Polarized Superfluids: The Fulde-Ferrell-Larkin-Ovchinnikov State Reveals Itself *Phys. Rev. Lett.* **108** 225302

[27] Bolech C J, Heidrich-Meisner F, Langer S, McCulloch I P, Orso G and Rigol M 2012 Long-Time Behavior of the Momentum Distribution During the Sudden Expansion of a Spin-Imbalanced Fermi Gas in One Dimension *Phys. Rev. Lett.* **109** 110602

[28] Winkler K, Thalhammer G, Lang F, Grimm R, Denschlag J H, Daley A J, Kantian A, Büchler H P and Zoller P 2006 Repulsively bound atom pairs in an optical lattice *Nature* **441** 853

[29] Rosch A, Rasch D, Binz B and Vojta M 2008 Metastable Superfluidity of Repulsive Fermionic Atoms in Optical Lattices *Phys. Rev. Lett.* **101** 265301

[30] Heidrich-Meisner F, Manmana S R, Rigol M, Muramatsu A, Feiguin A E and Dagotto E 2009 Quantum distillation: Dynamical generation of low-entropy states of strongly correlated fermions in an optical lattice *Phys. Rev. A* **80** 041603

[31] Schneider U, Hackermüller L, Will S, Best T, Bloch I, Costi T A, Helmes R W, Rasch D and Rosch A 2008 Metallic and Insulating Phases of Repulsively Interacting Fermions in a 3D Optical Lattice *Science* **322** 1520

[32] Jördens R, Strohmaier N, Günter K, Moritz H and Esslinger T 2008 A mott insulator of fermionic atoms in an optical lattice *Nature* **455** 204–207

[33] Deuchert A, Sakmann K, Streltsov A I, Alon O E and Cederbaum L S 2012 Dynamics and symmetries of a repulsively bound atom pair in an infinite optical lattice *Phys. Rev. A* **86** 013618

[34] Vidal G 2004 Efficient Simulation of One-Dimensional Quantum Many-Body Systems *Phys. Rev. Lett.* **93** 040502

[35] Daley A J, Kollath C, Schollwöck U and Vidal G 2004 Time-dependent density-matrix renormalization-group using adaptive effective hilbert spaces *J. Stat. Mech.* **2004** P04005

[36] White S R and Feiguin A E 2004 Real-time evolution using the density matrix renormalization group *Phys. Rev. Lett.* **93** 076401

[37] Schmitteckert P 2004 Nonequilibrium electron transport using the density matrix renormalization group method *Phys. Rev. B* **70** 121302(R)

[38] Schollwöck U 2011 The density-matrix renormalization group in the age of matrix product states *Annals of Physics* **326** 96–192

[39] Lahini Y, Verbin M, Huber S D, Bromberg Y, Pugatch R and Silberberg Y 2012 Quantum walk of two interacting bosons *Phys. Rev. A* **86** 011603

[40] Muth D, Petrosyan D and Fleischhauer M 2012 Dynamics and evaporation of defects in Mott-insulating clusters of boson pairs *Phys. Rev. A* **85** 013615

[41] Jin L and Song Z 2011 Perfect coherent shift of bound pairs in strongly correlated systems *Phys. Rev. A* **83** 052102

[42] Wootters W K 1998 Entanglement of Formation of an Arbitrary State of Two Qubits *Phys. Rev. Lett.* **80** 2245–2248

[43] Ramšak A, Mravlje J, Rejec T and Lautar A 2009 Entanglement of electron pairs extracted from a many-body system *EPL* **86** 40003

[44] Fano U 1957 Description of States in Quantum Mechanics by Density Matrix and Operator Techniques *Rev. Mod. Phys.* **29** 74–93

[45] Amico L, Osterloh A, Plastina F, Fazio R and Massimo Palma G 2004 Dynamics of entanglement in one-dimensional spin systems *Phys. Rev. A* **69** 022304

[46] Amico L, Fazio R, Osterloh A and Vedral V 2008 Entanglement in many-body systems *Rev. Mod. Phys.* **80** 517–576

[47] Vollbrecht K G H and Cirac J I 2007 Delocalized Entanglement of Atoms in Optical Lattices *Phys. Rev. Lett.* **98** 190502

[48] Cramer M, Plenio M B and Wunderlich H 2011 Measuring Entanglement in Condensed Matter Systems *Phys. Rev. Lett.* **106** 020401

[49] Levine G C, Friedman B A and Bantegui M J 2011 Detecting many-body entanglement in noninteracting ultracold atomic Fermi gases *Phys. Rev. A* **83** 013623

[50] Lignier H, Sias C, Ciampini D, Singh Y, Zenesini A, Morsch O and Arimondo E 2007 Dynamical Control of Matter-Wave Tunneling in Periodic Potentials *Phys. Rev. Lett.* **99** 220403

[51] Roos C F, Lancaster G P T, Riebe M, Häffner H, Hänsel W, Gulde S, Becher C, Eschner J, Schmidt-Kaler F and Blatt R 2004 Bell States of Atoms with Ultralong Lifetimes and Their Tomographic State Analysis *Phys. Rev. Lett.* **92** 220402

[52] Weitenberg C, Endres M, Sherson J F, Cheneau M, Schauß P, Fukuhara T, Bloch I and Kuhr S 2011 Single-spin addressing in an atomic Mott insulator *Nature* **471** 319

[53] Weitenberg C 2011 *Single-Atom Resolved Imaging and Manipulation in an Atomic Mott Insulator* Ph.D. thesis Ludwig-Maximilians-Universität München

[54] Löwdin P O 1955 Quantum theory of many-particle systems. I. Physical interpretations by means of density matrices, natural spin-orbitals, and convergence problems in the method of configurational interaction *Phys. Rev.* **97** 1474–1489

[55] Valiente M and Petrosyan D 2008 Two-particle states in the Hubbard model *Journal of Physics B: Atomic, Molecular and Optical Physics* **41** 161002